ammonia would react directly with compounds **4a** and **4b**, and a dissociative path D, in which ammonia would react with a 14-electron complex formed after dissociation of olefin (Scheme 5). The rates of decay of the pentene complex **4b** were measured by ^{31}P NMR spectroscopy with varied amounts of olefin and ratios of ammonia to olefin (data and plot are shown in figs. S1 and S2 and table S1). The observable rate constants, k_{obs}, predicted for reaction by associative path C (Eq. 1) and dissociative path D (Eq. 2), were derived with the steady state approximation. For path C, the observed rate constant would be independent of the concentration of olefin, but for path D, a plot of $1/k_{obs}$ versus the ratio of olefin to ammonia is predicted to be linear with a nonzero intercept. The reactions were clearly slower at higher concentrations of olefin, and a plot of $1/k_{obs}$ versus the ratio of olefin to ammonia was found to be linear with a positive slope ($0.20 \times 10^{-4} \pm 0.01 \times 10^{-4}$ s^{-1}) and a nonzero y intercept ($0.65 \times 10^{-4} \pm 0.16 \times 10^{-4}$ s). These data suggest that olefin dissociation is the first step in the reaction, and, if so, the y intercept of this double reciprocal plot would correspond to the inverse of the rate constant for dissociation of olefin.

$$\frac{1}{k_{obs}} = \frac{k_{-1}}{k_1 k_2[\text{ammonia}]} + \frac{1}{k_1[\text{ammonia}]} \quad (1)$$

$$\frac{1}{k_{obs}} = \frac{k_{-1}[\text{pentene}]}{k_1 k_2[\text{ammonia}]} + \frac{1}{k_1} \quad (2)$$

Because substitution reaction of square-planar d^8 complexes typically proceed associatively, and because the reactions could occur by more complex pathways with multiple equilibria preceding N-H bond cleavage, we conducted further experiments to test whether the reaction was initiated by dissociation of olefin. The pentene in complex **4b** is displaced by ethylene to form ethylene complex **4c**. If the reactions of **4b** occur dissociatively, then the rate constants for dissociation of pentene obtained from the reaction of **4b** with ethylene and from the reaction of **4b** with ammonia should be the same.

Consistent with dissociative reactions of **4b**, the reaction of **4b** with ethylene was independent of the concentration of ethylene or 0.03 to 0.3 M added pentene; all reactions occurred with rate constants within 3% of the mean value of 1.6×10^{-3}. Moreover, this mean value is well within experimental error of the value of k_1 (1.5×10^{-3}) measured for the reaction of ammonia with **4b**.

The identification of an iridium complex that undergoes oxidative addition of ammonia and the elucidation of key thermodynamic and mechanistic aspects of the reaction advance our understanding of how to cleave N-H bonds under mild conditions. We anticipate that this understanding will accelerate the development of catalytic chemistry that parallels the existing reactions of hydrogen, hydrocarbons, silanes, and boranes but begins with oxidative addition of the N-H bond of abundant and inexpensive ammonia.

References and Notes

1. G. B. Kauffman, in *Coordination Chemistry: A Century of Progress*. (American Chemical Society Symposium Series, Washington, DC, 1994), vol. 565, pp. 3–34.
2. Two reactions of ammonia are among the top 10 challenges for catalysis listed in this article: J. Haggin, *Chem. Eng. News*. **71**, 23 (1993).
3. For a reaction of an Ir(I) complex with ammonia to form an insoluble product containing hydrides and bridging amides, as characterized by solid-state IR and ^{1}H NMR spectroscopy and derivatization, see A. L. Casalnuovo, J. C. Calabrese, D. Milstein, *Inorg. Chem.* **26**, 971 (1987).
4. For the protonolysis of a hydride ligand on a group IV metal complex, presumably after coordination of the ammonia ligand, see G. L. Hillhouse, J. E. Bercaw, *J. Am. Chem. Soc.* **106**, 5472 (1984).
5. For an example of a reaction of ammonia with a cluster to form a product in low yield that was formulated by ^{1}H NMR spectroscopy to contain a bridging hydride and bridging amide, see E. G. Bryan, B. F. G. Johnson, J. Lewis, *J. Chem. Soc. Dalton Trans.* **1977**, 1328 (1977).
6. F. L. Joslin, M. P. Johnson, J. T. Mague, D. M. Roundhill, *Organometallics* **10**, 2781 (1991).
7. A. W. Kaplan, J. C. M. Ritter, R. G. Bergman, *J. Am. Chem. Soc.* **120**, 6828 (1998).
8. J. Campora, P. Palma, D. del Rio, M. M. Conejo, E. Alvarez, *Organometallics* **23**, 5653 (2004).
9. D. Conner, K. N. Jayaprakash, T. R. Cundari, T. B. Gunnoe, *Organometallics* **23**, 2724 (2004).
10. H. E. Bryndza, W. Tam, *Chem. Rev.* **88**, 1163 (1988).
11. J. R. Fulton, A. W. Holland, D. J. Fox, R. G. Bergman, *Acc. Chem. Res.* **35**, 44 (2002).
12. J. R. Fulton, S. Sklenak, M. W. Bouwkamp, R. G. Bergman, *J. Am. Chem. Soc.* **124**, 4722 (2002).
13. D. J. Fox, R. G. Bergman, *Organometallics* **23**, 1656 (2004).
14. M. Kanzelberger, B. Singh, M. Czerw, K. Krogh-Jespersen, A. S. Goldman, *J. Am. Chem. Soc.* **122**, 11017 (2000).
15. D. Morales-Morales, D. W. Lee, Z. Wang, C. M. Jensen, *Organometallics* **20**, 1144 (2001).
16. M. Kanzelberger *et al.*, *J. Am. Chem. Soc.* **125**, 13644 (2003).
17. K. Krogh-Jesperson *et al.*, *J. Am. Chem. Soc.* **124**, 10797 (2002).
18. N. A. Al-Salem, H. D. Empsall, R. Markham, B. L. Shaw, B. Weeks, *J. Chem. Soc. Dalton Trans.* **1979**, 1972 (1979).
19. M. A. McLoughlin, R. J. Flesher, W. C. Kaska, H. A. Mayer, *Organometallics* **13**, 3816 (1994).
20. Materials and methods, including the details of the synthesis of the olefin complexes, are available as supporting material on *Science* Online.
21. J. F. Riehl, Y. Jean, O. Eisenstein, M. Pelissier, *Organometallics* **11**, 729 (1992).
22. J. F. Hartwig, R. G. Bergman, R. A. Andersen, *J. Am. Chem. Soc.* **113**, 3404 (1991).
23. J. Ruiz, V. Rodriguez, G. Lopez, P. A. Chaloner, P. B. Hitchcock, *J. Chem. Soc. Dalton Trans.* **1997**, 4271 (1997).
24. M. Kanzelberger *et al.*, *J. Am. Chem. Soc.* **125**, 13644 (2003).
25. P. L. Holland, R. A. Andersen, R. G. Bergman, J. K. Huang, S. P. Nolan, *J. Am. Chem. Soc.* **119**, 12800 (1997).
26. H. A. Y. Mohammad *et al.*, *Organometallics* **21**, 5775 (2002).
27. H. D. Empsall *et al.*, *J. Chem. Soc. Chem. Commun.* **1977**, 589 (1977).
28. C. Crocker *et al.*, *J. Chem. Soc. Dalton Trans.* **1982**, 1217 (1982).
29. This method would detect deuterium in the ligand if it were present in 10% of the sample.

30. We thank the Department of Energy for funding. Structural data for compounds **4a** and **5** have been deposited in the Cambridge Crystallographic Data Centre under CCDC 260224 (**4a**) and 260225 (**5**), and can be obtained free of charge at www.ccdc.cam.ac.uk/conts/retrieving.html. We thank L. Bienen for editing of the manuscript.

Supporting Online Material

www.sciencemag.org/cgi/content/full/307/5712/1080/DC1
Materials and Methods
Figs. S1 to S5
Tables S1 to S6
References and Notes

1 December 2004; accepted 12 January 2005
10.1126/science.1109389

Efficient Bipedal Robots Based on Passive-Dynamic Walkers

Steve Collins,[1] Andy Ruina,[2]* Russ Tedrake,[3] Martijn Wisse[4]

Passive-dynamic walkers are simple mechanical devices, composed of solid parts connected by joints, that walk stably down a slope. They have no motors or controllers, yet can have remarkably humanlike motions. This suggests that these machines are useful models of human locomotion; however, they cannot walk on level ground. Here we present three robots based on passive-dynamics, with small active power sources substituted for gravity, which can walk on level ground. These robots use less control and less energy than other powered robots, yet walk more naturally, further suggesting the importance of passive-dynamics in human locomotion.

Most researchers study human locomotion by observing people as they walk, measuring joint angles and ground reaction forces (*1*). Our approach is different: We study human locomotion by designing and testing walking machines that we compare to humans in terms of morphology, gait appearance, energy use, and control.

Previous bipedal robots with humanlike forms have demonstrated smooth, versatile motions (*2–5*). These impressive robots are based on the mainstream control paradigm, namely, precise joint-angle control. For the study of human walking, this control paradigm is unsatisfactory, because it requires actuators with higher precision and frequen-

cy response than human muscles have (*6*) and requires an order of magnitude more energy. To address these issues, passive-dynamic walkers (Fig. 1) were proposed as a new design and control paradigm (*7*). In contrast to mainstream robots, which actively control every joint angle at all times, passive-dynamic walkers do not control any joint angle at any time. Although these walkers have no actuation or control, they can walk downhill with startlingly humanlike gaits (*8*).

To demonstrate that the humanlike properties of passive-dynamic machines are not dependent on gravitational power, but rather extend to level-ground walking, we built three powered walking robots (Fig. 2) at three institutions, substituting gravitational power with simple actuation. The Cornell biped (Fig. 2A) is based on the passive device in Fig. 1D and is powered by electric motors with springs that drive ankle push-off. It has five internal degrees of freedom (two ankles, two knees, and a hip), each arm is mechanically linked to the opposite leg, and the small body is kinematically constrained so that its midline bisects the hip angle. The Delft biped (Fig. 2B) has a similar morphology, but it is powered by pneumatic hip actuation and has a passive ankle. The Massachusetts Institute of Technology (MIT) learning biped (Fig. 2C) is based on the simpler ramp-walkers in Fig. 1, A and B. It has six internal degrees of freedom (two servo motors in each ankle and two passive hips), each arm is mechanically linked to the opposite leg, the body hangs passively, and it uses reinforcement learning to automatically acquire a control policy. The supporting online movies show these robots walking and the supporting online text describes their construction details (*9*).

The Cornell biped is specifically designed for minimal energy use. The primary energy losses for humans and robots walking at a constant speed are due to dissipation when a foot hits the ground and to active braking by the actuators (negative work). The Cornell design demonstrates that it is possible to completely avoid this negative actuator work. The only work done by the actuators is positive: The left ankle actively extends when triggered by the right foot hitting the ground, and vice versa. The hip joint is not powered, and the knee joints only have latches. The average mechanical power (*10*) of the two ankle joints is about 3 W, almost identical to the scaled gravitational power consumed by the passive-dynamic machine on which it is based (*8*). Including electronics, microcontroller, and actuators, the Cornell biped consumes 11 W (*11*).

To compare efficiency between humans and robots of different sizes, it is convenient to use the dimensionless specific cost of transport, c_t = (energy used)/(weight × distance traveled). In order to isolate the effectiveness of the mechanical design and controller from the actuator efficiency, we distinguish between the specific energetic cost of transport, c_{et}, and the specific mechanical cost of transport, c_{mt}. Whereas c_{et} uses the total energy consumed by the system (11 W for the Cornell biped), c_{mt} only considers the positive mechanical work of the actuators (3 W for the Cornell biped). The 13-kg Cornell biped walking at 0.4 m/s has $c_{et} \approx 0.2$ and $c_{mt} \approx 0.055$. Humans are similarly energy effective, walking with $c_{et} \approx 0.2$, as estimated by the volume of oxygen they consume (V_{O_2}), and $c_{mt} \approx 0.05$ (*12*–*14*). Measurement of actuator work on the Delft biped yields $c_{mt} \approx 0.08$. Based on the small slopes that it descends when passive, we estimate the MIT biped to have $c_{mt} \geq 0.02$. Although the MIT and Delft bipeds were not specifically designed for low-energy use, both inherit energetic features from the passive-dynamic walkers on which they are based. By contrast, we estimate the state-of-the-art Honda humanoid Asimo to have $c_{et} \approx 3.2$ and $c_{mt} \approx 1.6$ (*15*). Thus Asimo, perhaps representative of joint-angle controlled robots, uses at least 10 times the energy (scaled) of a typical human.

Control algorithms for state-of-the-art, level-ground walking robots are typically complex, requiring substantial real-time computation. In contrast, the Delft and Cornell bipeds walk with primitive control algorithms. Their only sensors detect ground contact, and their only motor commands are on/off signals issued once per step. In addition to powering the motion, hip actuation in the Delft biped also improves fore-aft robustness against large disturbances by swiftly placing the swing leg in front of the robot before it has a chance to fall forward (*16*, *17*).

The MIT biped (Fig. 2C) is designed to test the utility of motor learning on a passive-dynamic mechanical design. The goal of the learning is to find a control policy that

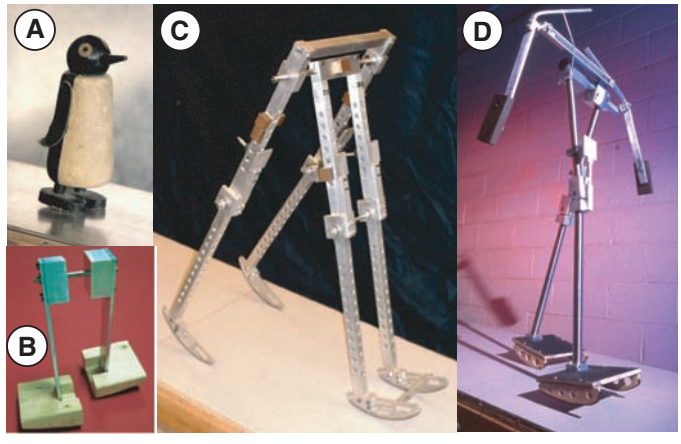

Fig. 1. "Ramp-walking," "downhill," "unpowered," or "passive-dynamic" machines. Our powered bipeds are based on these passive designs. (**A**) The Wilson "Walkie" (*27*). (**B**) MIT's improved version (*28*). Both (A) and (B) walk down a slight ramp with the "comical, awkward, waddling gait of the penguin" (*27*). (**C**) Cornell copy (*29*) of McGeer's capstone design (*7*). This four-legged "biped" has two pairs of legs, an inner and outer pair, to prevent falling sideways. (**D**) The Cornell passive biped with arms [photo: H. Morgan]. This walker has knees and arms and is perhaps the most humanlike passive-dynamic walker to date (*8*).

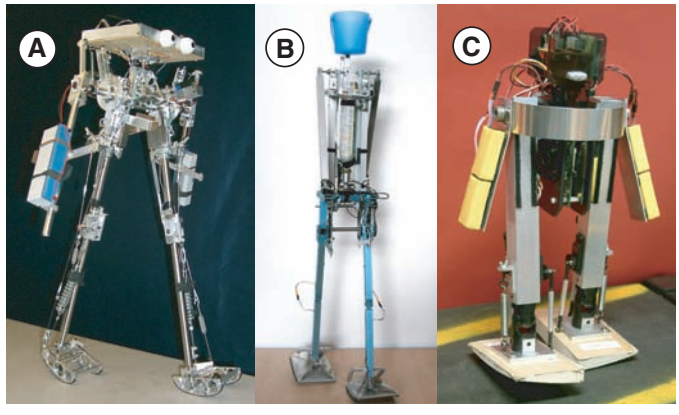

Fig. 2. Three level-ground powered walking robots based on the ramp-walking designs of Fig. 1. (**A**) The Cornell biped. (**B**) The Delft biped. (**C**) The MIT learning biped. These powered robots have motions close to those of their ramp-walking counterparts as seen in the supporting online movies (movies S1 to S3). Information on their construction is in the supporting online text (*9*).

[1]Mechanical Engineering, University of Michigan, Ann Arbor, MI 48104, USA. [2]Theoretical and Applied Mechanics, Cornell University, Ithaca, NY 14853, USA. [3]Brain and Cognitive Sciences and Center for Bits and Atoms, Massachusetts Institute of Technology, Cambridge, MA 02139, USA. [4]Mechanical Engineering, Delft University of Technology, NL-2628 CD Delft, Netherlands.

*To whom correspondence should be addressed. E-mail: ruina@cornell.edu

stabilizes the robot's trajectory on level terrain using the passive ramp-walking trajectory as the target. The robot acquires a feedback control policy that maps sensors to actions using a function approximator with 35 parameters. With every step that the robot takes, it makes small, random changes to the parameters and measures the change in walking performance. This measurement yields a noisy sample of the relation between the parameters and the performance, called the performance gradient, on each step. By means of an actor-critic reinforcement learning algorithm (*18*), measurements from previous steps are combined with the measurement from the current step to efficiently estimate the performance gradient on the real robot despite sensor noise, imperfect actuators, and uncertainty in the environment. The algorithm uses this estimate in a real-time gradient descent optimization to improve the stability of the step-to-step dynamics (Fig. 3). The robot's actuators are mounted so that when they are commanded to their zero position, the robot imitates its passive counterpart. Starting from this zero policy, the learning system quickly and reliably acquires an effective control policy for walking, using only data taken from the actual robot (no simulations), typically converging in 10 min or ~600 steps. Figure 3 illustrates that the learned control policy not only achieves the desired trajectory but is also robust to disturbances. The robot can start, stop, steer, and walk forward and backward at a small range of speeds. This learning system works quickly enough that the robot is able to continually adapt to the terrain (e.g., bricks, wooden tiles, and carpet) as it walks.

Each of the robots here has some design features that are intended to mimic humans. The Cornell and Delft bipeds use anthropomorphic geometry and mass distributions in their legs and demonstrate ankle push-off and powered leg swinging, both present in human walking (*14*, *19*). They do not use high-power or high-frequency actuation, which are also unavailable to humans. These robots walk with humanlike efficiency and humanlike motions (Fig. 4 and movies S1 to S3). The motor learning system on the MIT biped uses a learning rule that is biologically plausible at the neural level (*20*). The learning problem is formulated as a stochastic optimal feedback control problem; there is emerging evidence that this formulation can also describe biological motor learning (*21*).

The Cornell and Delft bipeds demonstrate that walking can be accomplished with extremely simple control. These robots do not rely on sophisticated real-time calculations or on substantial sensory feedback such as from continuous sensing of torques, angles, or attitudes. This implies that steady-state human walking might require only simple control as well; the sequencing of human joint-angles in time might be determined as much by morphology as by motor control. We note that no other robots have done particularly better at generating humanlike gaits even when using high-performance motors, a plethora of sensors, and sophisticated control.

In theory, pushing off just before heel-strike requires about one-fourth the energy of pushing off just after heel-strike (*22*, *23*), so the Cornell robot was initially designed with this preemptive push-off strategy. Initial push-off resulted in both higher torque demands on the motor and a high sensitivity to push-off timing that our primitive control system could not reliably stabilize. Humans seem to solve both of these problems without a severe energy penalty by using a double support phase that overlaps push-off and heel-strike. These issues must also be addressed in the design of advanced foot prostheses.

The success of the Delft robot at balancing using ankles that kinematically couple

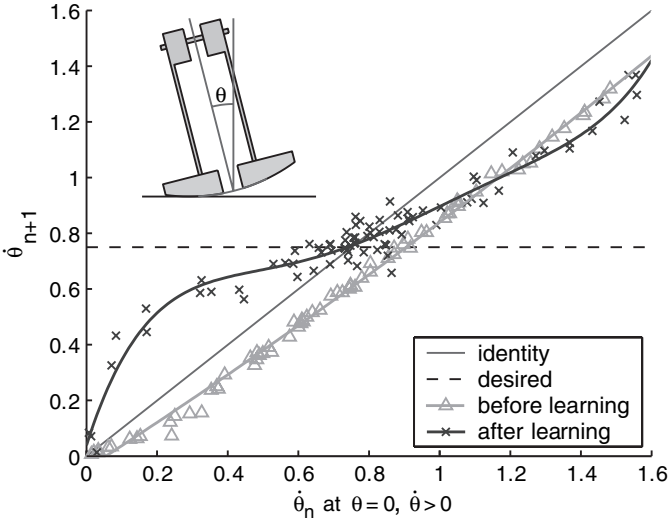

Fig. 3. Step-to-step dynamics of the MIT biped walking in place on a level surface, before (△) and after (x) learning. Shown is the roll angular velocity when the right foot collides with the ground ($\theta = 0$, $\dot{\theta} > 0$) at step $n + 1$ versus step n. Intersections of the plots with the solid identity line are fixed points. The horizontal dashed line is the theoretical ideal; the robot would reach $\dot{\theta} = 0.75\ s^{-1}$ in one step. This ideal cannot be achieved due to limitations in the controllability of the actuation system. On a level surface, before learning, the robot loses energy on every step ($\dot{\theta}_{n+1} < \dot{\theta}_n$), eventually coming to rest at $\dot{\theta} = 0$. After learning, the robot quickly converges near $\dot{\theta} = 0.75\ s^{-1}$ for $0 \le \dot{\theta}_0 \le 1.7\ s^{-1}$.

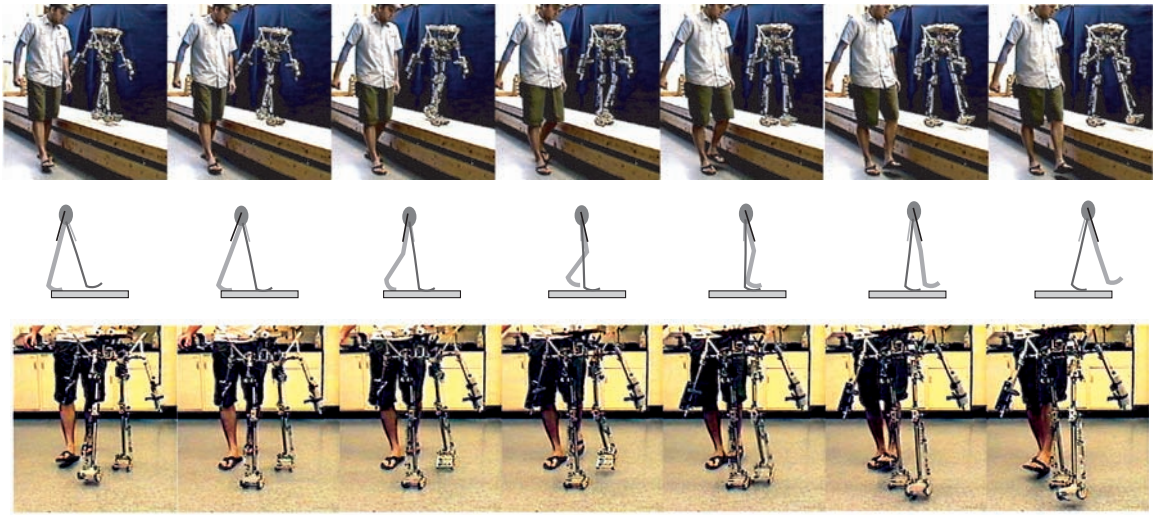

Fig. 4. Two sets of video stills of the Cornell ankle-powered biped walking on a level surface next to a person. A little less than one step is shown at 7.5 frames/s. Both the robot and the person are walking at about 1 step/s. The stick figure indicates the leg angles for the corresponding video stills; the right arm and leg are darker than the left.

leaning to steering hints that humans could similarly use a simple coupling between lean and lateral foot placement to aid balance. Furthermore, simulations used in the development of the Delft robot showed that the swift swing-leg motion not only increased fore-aft stability but also increased lateral stability. Indeed, the physical robot was not able to balance laterally without sufficient fore-aft swing-leg actuation. This highlights the possible coupling between lateral and sagittal balance in human walking.

The MIT biped shows that the efficiency of motor learning can be strongly influenced by the mechanical design of the walking system, both in robots and possibly in humans. Previous attempts at learning control for bipedal robots have required a prohibitively large number of learning trials in simulation (*24*) or a control policy with predefined motion primitives on the robot (*25*). By exploiting the natural stability of walking trajectories on the passive-dynamic walker, our robot was able to learn in just a few minutes without requiring any initial control knowledge. We also found that it was possible to estimate the walking performance gradient by making surprisingly small changes to the control parameters, allowing the robot to continue walking naturally as it learns. This result supports the use of actor-critic reinforcement learning algorithms as models for biological motor learning.

The conclusion that natural dynamics may largely govern locomotion patterns was already suggested by passive-dynamic machines. A common misconception has been that gravity power is essential to passive-dynamic walking, making it irrelevant to understanding human walking. The machines presented here demonstrate that there is nothing special about gravity as a power source; we achieve successful walking using small amounts of power added by ankle or hip actuation.

We expect that humanoid robots will be improved by further developing control of passive-dynamics–based robots and by paying closer attention to energy efficiency and natural dynamics in joint-controlled robots (*26*). Whatever the future of humanoid robots, the success of human mimicry demonstrated here suggests the importance of passive-dynamic concepts in understanding human walking.

References and Notes

1. D. A. Winter, *The Biomechanics and Motor Control of Human Gait* (Univ. of Waterloo Press, Waterloo, Ontario, Canada, 1987).
2. I. Kato *et al.*, *Proc. CISM-IFToMM Theory and Practice of Robots and Manipulators* (Udine, Italy, 1973), pp. 12–24.
3. Y. Sakagami *et al.*, *Proc. IEEE/Robotics Society of Japan (RSJ) Int. Conf. Intell. Robots Syst.* (IEEE/RSJ, Lausanne, Switzerland, 2002), pp. 2478–2483.
4. C. Chevallereau *et al.*, *IEEE Control Syst. Mag.* **23**, 57 (2003).
5. F. Pfeiffer, K. Löffler, M. Gienger, *Proc. IEEE Int. Conf. Robotics Automation* (IEEE, Washington, DC, 2002), pp. 3129–3135.
6. F. Zajac, *Crit. Rev. Biomed. Eng.* **17**, 359 (1989).
7. T. McGeer, *Int. J. Robotics Res.* **9**, 62 (1990).
8. S. H. Collins, M. Wisse, A. Ruina, *Int. J. Robot. Res.* **20**, 607 (2001).
9. Supporting online movies and text are available at *Science* Online.
10. Mechanical power is defined here as net positive mechanical work at the joints $= \int_0^T \sum [\omega_j M_j]^+ dt/T$ where T is the period of one step, ω_j is the relative angular velocity at one joint, M_j is the torque across that joint, $[x]^+ = x$ if $x > 0$ and 0 otherwise, and the sum is over all the joints. Because only the ankle does positive work on the Cornell robot, this can be measured by measuring the foot force as the ankle extends during push-off.
11. For the Cornell robot, total power was measured by averaging the voltage across a 1-ohm resistor put in series with the battery.
12. E. Atzler, R. Herbst, *Pflueg. Arch. Gesamate Physiol.* **215**, 291 (1927).
13. N. H. Molen, R. H. Rozendal, W. Boon, *Proc. K. Ned. Akad. Wet. Ser. C* **75**, 305 (1972).
14. J. M. Donelan, R. Kram, A. D. Kuo, *J. Exp. Biol.* **205**, 3717 (2002).
15. Honda's ASIMO can walk at a variety of speeds, kick balls, and even climb stairs. It weighs 510 N, can walk at speeds up to 1.6 km hour^{-1}, and drains a 38.4-V, 10–A-hour battery in about 30 min (http://world.honda.com/ASIMO/). Using these numbers, we estimate $c_{et} \approx 3.2$ and, assuming a 50% drive train efficiency, $c_{mt} \approx 1.6$.
16. M. Wisse, J. van Frankenhuyzen, *Proc. Conf. Adaptive Motion Anim. Machines* (Kyoto, Japan, 2003).
17. M. Wisse, A. L. Schwab, R. Q. van der Linde, F. C. T. van der Helm, *IEEE Trans. Robot.*, in press.
18. R. Tedrake, T. W. Zhang, M. Fong, H. S. Seung, *Proc. IEEE/RSJ Int. Conf. Intell. Robots Syst.* (IEEE/RSJ, Sendai, Japan, 2004).
19. T. McGeer, *J. Theor. Biol.* **163**, 277 (1993).
20. H. Seung, *Neuron* **40**, 1063 (2003).
21. E. Todorov, *Nature Neurosci.* **5**, 1226 (2002).
22. A. D. Kuo, *J. Biomech. Eng.* **124**, 113 (2002).
23. A. Ruina, J. Bertram, M. Srinivasan, *J. Theor. Biol.*, in press.
24. H. Benbrahim, J. A. Franklin, *Robot. Auton. Syst.* **22**, 283 (1997).
25. A. Kun, W. T. Miller III, *Proc. IEEE Int. Conf. Robotics Automation* (IEEE, Minneapolis, MN, 1996).
26. J. Pratt, thesis, Massachusetts Institute of Technology (2000).
27. J. E. Wilson, U.S. Patent 2,140, 275; available at www.tam.cornell.edu/~ruina/hplab/.
28. R. Tedrake, T. W. Zhang, M. Fong, H. S. Seung, *Proc. IEEE Int. Conf. Robotics Automation* (IEEE, New Orleans, LA, 2004).
29. M. Garcia, A. Chatterjee, A. Ruina, *Dyn. Stabil. Syst.* **15**, 75 (2000).

30. The Cornell robot was developed by S.C. with suggestions from A.R.; the Delft robot was developed by M.W. and J. van Frankenhuyzen on an Stichting Technische Wetenschappen grant, with help from A. Schwab; and the MIT robot was developed by R.T. and T. Weirui Zhang with help from M.-f. Fong and D. Tan in the lab of H. Sebastian Seung. A.R. and S.C. were funded by an NSF Biomechanics grant. R.T. was funded by the Packard Foundation and the NSF. The text was improved by comments from N. Agnihotri, C. Atkeson, J. Burns, A. Chatterjee, M. Coleman, J. Grizzle, P. Holmes, I. ten Kate, A. Kun, A. Kuo, Y. Loewenstein, S. van Nouhuys, D. Paluska, A. Richardson, S. Seung, M. Srinivasan, S. Strogatz, and N. Sydor.

Supporting Online Material

www.sciencemag.org/cgi/content/full/307/5712/1082/DC1
Materials and Methods
SOM Text
Movies S1 to S3
References and Notes

22 November 2004; accepted 26 January 2005
10.1126/science.1107799

Terrestrial Gamma-Ray Flashes Observed up to 20 MeV

David M. Smith,[1]* Liliana I. Lopez,[2] R. P. Lin,[3] Christopher P. Barrington-Leigh[4]

Terrestrial gamma-ray flashes (TGFs) from Earth's upper atmosphere have been detected with the Reuven Ramaty High Energy Solar Spectroscopic Imager (RHESSI) satellite. The gamma-ray spectra typically extend up to 10 to 20 megaelectron volts (MeV); a simple bremsstrahlung model suggests that most of the electrons that produce the gamma rays have energies on the order of 20 to 40 MeV. RHESSI detects 10 to 20 TGFs per month, corresponding to ~50 per day globally, perhaps many more if they are beamed. Both the frequency of occurrence and maximum photon energy are more than an order of magnitude higher than previously known for these events.

Terrestrial gamma-ray flashes (TGFs) were unexpectedly detected from Earth's atmosphere by the Burst and Transient Source Experiment (BATSE) on the Compton Gamma-Ray Observatory (CGRO), a NASA satellite in low-Earth orbit between 1991 and 2000. Each BATSE TGF (*1*) lasted between a fraction of a millisecond and several milliseconds, shorter than all other transient gamma-ray phenomena observed from space. Since they were first detected, it has also been noticed that TGFs had a harder energy spectrum (higher average energy per photon) than any of these other phenomena (*1*).

Fishman *et al.* (*1*) immediately interpreted the TGFs as high-altitude electrical discharges and found a correlation with thunderstorms.

[1]Physics Department and Santa Cruz Institute for Particle Physics, University of California, Santa Cruz, 1156 High Street, Santa Cruz, CA 95064, USA. [2]Astronomy Department and Space Sciences Laboratory, University of California, Berkeley, Berkeley, CA 94720, USA. [3]Physics Department and Space Sciences Laboratory, University of California, Berkeley, Berkeley, CA 94720, USA. [4]University of British Columbia, 2329 West Mall Vancouver, BC V6T 1Z4 Canada.

*To whom correspondence should be addressed. E-mail: dsmith@scipp.ucsc.edu